nature neuroscience

RESOURCE

Neuronal activity modifies the DNA methylation landscape in the adult brain

Junjie U Guo[1,2], Dengke K Ma[1,3], Huan Mo[4], Madeleine P Ball[5], Mi-Hyeon Jang[1,3], Michael A Bonaguidi[1,3], Jacob A Balazer[6], Hugh L Eaves[4], Bin Xie[7], Eric Ford[8], Kun Zhang[9], Guo-li Ming[1–3], Yuan Gao[1,7] & Hongjun Song[1–3]

DNA methylation has been traditionally viewed as a highly stable epigenetic mark in postmitotic cells. However, postnatal brains appear to show stimulus-induced methylation changes, at least in a few identified CpG dinucleotides. How extensively the neuronal DNA methylome is regulated by neuronal activity is unknown. Using a next-generation sequencing–based method for genome-wide analysis at single-nucleotide resolution, we quantitatively compared the CpG methylation landscape of adult mouse dentate granule neurons *in vivo* before and after synchronous neuronal activation. About 1.4% of 219,991 CpGs measured showed rapid active demethylation or *de novo* methylation. Some modifications remained stable for at least 24 h. These activity-modified CpGs showed a broad genomic distribution with significant enrichment in low-CpG density regions, and were associated with brain-specific genes related to neuronal plasticity. Our study implicates modification of the neuronal DNA methylome as a previously underappreciated mechanism for activity-dependent epigenetic regulation in the adult nervous system.

Epigenetic modifications of chromatin molecules, including genomic DNA and histone proteins, are critical in orchestrating the transcriptome of different cell types and their developmental potentials[1–3]. In contrast to readily reversible histone modifications, DNA methylation has been generally regarded as a highly stable epigenetic mark in differentiated cells to ensure transcriptional gene silencing and maintain cell type identity[1,2,4]. DNA methylation, catalyzed by DNA methyltransferases (DNMTs), occurs on cytosine bases almost exclusively in CpG dinucleotides in somatic cells. Although clustered 5-methylcytosines (5mCs) are well-established transcriptional repressors in gene silencing and inactivation of endogenous transposable elements[5], emerging evidence suggests diverse roles of DNA methylation in various contexts, including promoting gene expression[2,6–8]. In addition, 5-hydroxymethylcytosines (5hmCs) are present in the genomic DNA of mature neurons, although their potential function in gene regulation remains largely unknown[4,9].

How experience-driven transient synaptic activity leads to long-lasting modifications of neural circuits and neuronal properties is a longstanding question. Emerging evidence suggests the importance of epigenetic regulation in activity-dependent mature brain functions[10–13], including synaptic plasticity[13], learning and memory[14], circadian rhythm[15], drug addiction[16] and adult neurogenesis[17]. Interestingly, recent studies have implicated CpG methylation changes in neural plasticity[18–21]. Deletion of *Dnmt1* and *Dnmt3a* in mouse forebrain excitatory neurons leads to deficits in neuronal morphology, synaptic plasticity, and learning and memory[20]. *Dnmt3a* is also critical for emotional behavior and spine plasticity in adult mouse nucleus accumbens[21]. Recent studies have identified several specific CpGs that could be acutely modified by neuronal activity or behavior in postnatal neural tissues[17,22–29]. For example, neuronal stimulation induces *Gadd45b* (growth arrest and DNA-damage-inducible 45β)-dependent DNA demethylation at specific promoters of *Bdnf* (brain-derived neurotrophic factor) and *Fgf1* (fibroblast growth factor 1) in the adult mouse dentate gyrus[17]. However, the scope and global properties of activity-induced changes in neuronal DNA methylation remain unknown.

Here we used an improved genome-wide profiling method for analysis of the DNA methylome of dentate granule neurons in the adult mouse hippocampus *in vivo*, before and after synchronous neuronal activation. We identified many changes in CpG methylation status in response to neuronal stimulation. Bioinformatic analysis further revealed unexpected properties of the genomic distribution of these activity-modified CpGs. Our study provides, to our knowledge, the first global view of how the DNA methylation landscape of mature neurons is rapidly modified in response to external stimuli *in vivo* and implicates active DNA modifications as a general mechanism for activity-dependent epigenetic regulation in the adult brain.

[1]Institute for Cell Engineering, Johns Hopkins University School of Medicine, Baltimore, Maryland, USA. [2]The Solomon Snyder Department of Neuroscience, Johns Hopkins University School of Medicine, Baltimore, Maryland, USA. [3]Department of Neurology, Johns Hopkins University School of Medicine, Baltimore, Maryland, USA. [4]Center for the Study of Biological Complexity, Virginia Commonwealth University, Richmond, Virginia, USA. [5]Department of Genetics, Harvard Medical School, Cambridge, Massachusetts, USA. [6]Proofpoint Inc., Sunnyvale, California, USA. [7]Division of Genomics, Epigenomics and Bioinformatics, Lieber Institute for Brain Development, Baltimore, Maryland, USA. [8]Department of Radiation Oncology, Johns Hopkins University School of Medicine, Baltimore, Maryland, USA. [9]Department of Bioengineering, University of California at San Diego, La Jolla, California, USA. Correspondence should be addressed to H.S. (shongju1@jhmi.edu) or Y.G. (garygao@gmail.com).

Received 31 May; accepted 8 July; published online 28 August 2011; doi:10.1038/nn.2900

RESULTS

Activity-induced modification of neuronal DNA methylome

To determine the extent to which neuronal activity modifies the landscape of neuronal DNA methylation *in vivo*, we took a genome-wide approach to profile the DNA methylome of dentate granule cells in the adult mouse hippocampus with or without synchronous activation by electroconvulsive stimulation (ECS; **Supplementary Fig. 1**; see Online Methods), a procedure used to treat patients with drug-resistant depression[30]. At 0 h (E0; sham control), 4 h (E4) or 24 h (E24) after a single ECS, we purified genomic DNA from micro-dissected dentate gyrus tissues, which were highly enriched with postmitotic $NeuN^+Prox1^+$ dentate granule neurons (**Supplementary Fig. 1**; ref. 17). We used an improved methyl-sensitive cut counting (MSCC) method[7] to measure CpG methylation at single-nucleotide resolution (**Supplementary Fig. 2**). The methylation- and hydroxymethylation-sensitive restriction enzyme HpaII and its methylation-insensitive isoschizomer MspI used in the study recognize the same restriction site, CCGG. Locations of CCGGs largely reflect those of all CpGs in the mouse genome (**Supplementary Fig. 3**), allowing unbiased genome-scale analysis.

We constructed MSCC libraries and obtained a total of ~82 million uniquely mapped reads by next-generation sequencing (1.4 gigabase; **Supplementary Table 1**). The overall CpG methylation profiles of dentate granule neurons at E0, E4 and E24 are very similar (**Fig. 1a**), and the correlation between samples increases with sequencing depth (**Supplementary Fig. 4**). After excluding MSCC sites with low sequencing depth (<30 reads), we profiled 219,991 CpGs, representing ~1% of all CpGs in the mouse genome. Global methylation was comparable across all autosomes and X chromosomes, whereas the Y chromosome was hypermethylated (**Supplementary Fig. 5a**). A recent study has shown the presence of 5mCs and 5hmCs in the mammalian mitochondrial genome[31]. However, the neuronal mitochondrial genome is virtually unmethylated (**Supplementary Fig. 5a**), which is consistent with early findings[32]. Mapping of MSCC sites to their locations relative to associated genes showed a clear pattern of transcription start site (TSS) hypomethylation and gene body methylation (**Supplementary Fig. 5b**), which is also similar to findings from the human methylome[7,33,34]. In addition, exon-intron junctions showed consistent methylation patterns, as reported using a bisulfite sequencing-based method[33] (**Supplementary Fig. 5c**). These results collectively confirm the validity of our MSCC profiles.

Despite the global similarity, methylation changes were evident after neuronal activation, which outnumbered those that would be predicted by a Gaussian model of measurement variation with the same mean and variance (**Fig. 1a**). To validate detected methylation changes, we selected a set of 116 CpGs with different degrees of methylation changes (Δ_{MSCC}; either increase or decrease) for bisulfite sequencing using independent biological samples (**Fig. 1b**, **Supplementary Fig. 6a** and **Supplementary Table 2**). At Δ_{MSCC} ≥20%, our method achieved 94.6% specificity and 76.1% sensitivity (**Supplementary Fig. 6b**). We further used HpaII-digestion followed by quantitative PCR (HpaII-qPCR) to examine a set of 48 CpGs (Δ_{MSCC} ≥20%) in multiple individual mice (**Supplementary Table 3**). The interindividual variation in methylation at these CpGs was small (8 ± 4%; s.d.). There were also strong correlations for measurements between MSCC and bisulfite sequencing or HpaII-qPCR analysis (**Supplementary Figs. 7** and **8**). Using a cutoff of Δ_{MSCC} ≥20%, 1,892 and 1,158 CpGs showed activity-induced *de novo* methylation and demethylation at E4, respectively (**Supplementary Table 4**). The 3,050 CpGs represented in total ~1.4% of all profiled CpGs and likely constitute an underestimation, owing to the stringent depth requirement (≥30 reads) and cutoff for differential methylation (≥20%). For example, we confirmed CpG demethylation in *Nlgn3*, an autism-associated gene (<30 MSCC reads; **Supplementary Fig. 6c**). Thus, in contrast to the general belief that DNA methylation is a highly stable modification in terminally differentiated cells, a large number of CpGs were rapidly modified by neuronal activity in the adult brain.

To determine the duration of activity-induced CpG modifications, we obtained the neuronal DNA methylome profile at E24 (**Supplementary Table 4**). Whereas some of the methylation changes reverted to basal levels by E24, a significant number of CpGs showed sustained changes (**Fig. 2a–c**). Unsupervised hierarchical clustering analysis further revealed that the methylation pattern of these CpGs at E24 more closely resembled E4 than E0 (**Fig. 2b**). Specifically, 31% of activity-modified CpGs detected at E4 remained at their modified states at E24 (**Fig. 2c**). Thus, unlike activity-induced immediate early gene expression, which usually lasts up to several hours, activity-induced DNA modifications are relatively long-lasting.

Properties of activity-induced CpG modifications

To gain mechanistic insights into activity-induced CpG modifications, we subjected mice to pharmacological, genetic and behavioral manipulations and selected representative regions (putative promoters, exons, introns) for detailed bisulfite sequencing analysis (**Fig. 3**). As in HpaII-qPCR results, interindividual variation was small (7 ± 3%; s.d.; n = 124), and ECS-induced methylation changes were consistent among individual mice (**Fig. 3a**). Pretreatment of mice with

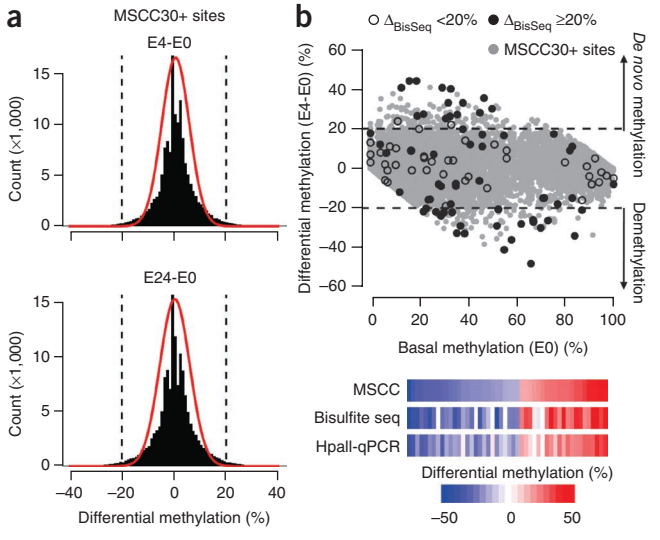

Figure 1 Modification of DNA methylation landscape in the adult dentate gyrus by neuronal activity. (**a**) Comparison of CpG methylation profiles of the dentate gyrus of adult mice at different time points after a single ECS. Shown are histograms of differential CpG methylation between sham control and 4 h after ECS ($\Delta_{MSCC,E4\text{-}E0}$; top) and between sham control and 24 h after ECS ($\Delta_{MSCC,E24\text{-}E0}$; bottom). Red lines represent Gaussian distributions with the same means and variances. Dashed lines represent ±20% cutoff. (**b**) A scatter plot of differential CpG methylation (E4-E0) at individual CpGs versus their basal methylation levels at E0 (MSCC estimates with 30 or more reads (MSCC30+); gray dots). Black dots indicate bisulfite analysis of selected MSCC sites for validation (filled, methylation change as measured by bisulfite analysis (Δ_{BisSeq}) ≥20%; open, Δ_{BisSeq} <20%). Below are heat maps of methylation changes detected by MSCC, bisulfite sequencing (seq) and HpaII-qPCR, from independent biological samples.

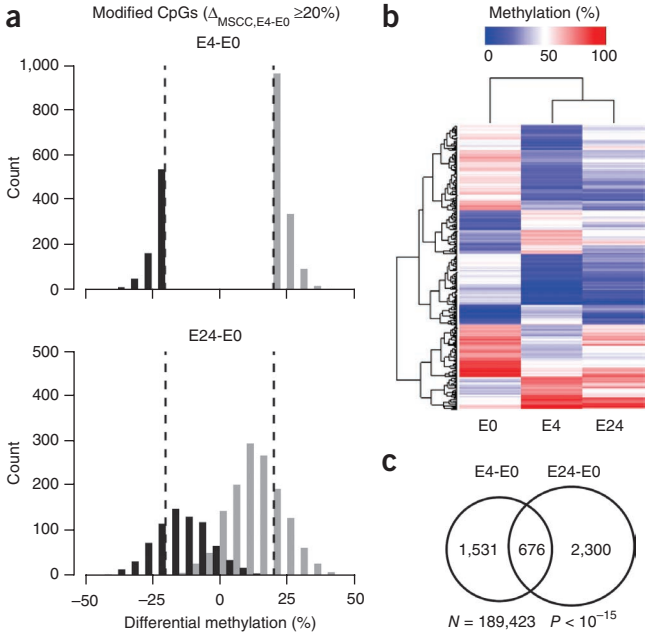

Figure 2 Persistence of activity-induced CpG modifications. (**a**) Histograms showing distributions of activity-modified CpGs ($\Delta_{MSCC,E4-E0}$ ≥20%) at E4 (top) and E24 (bottom). *De novo* methylated (black bars) and demethylated (gray bars) CpGs remain well segregated from E0 at E24. (**b**) Unsupervised hierarchical clustering of methylation levels of the top 500 MSCC sites with activity-induced modifications. The E24 profile is more similar to the E4 than to the E0, suggesting that activity-induced CpG modifications in mature neurons *in vivo* are fairly sustained. (**c**) Venn diagram showing highly significant overlapping between activity-modified CpGs identified at E4 and E24. Note that fewer MSCC sites (*N*) are used in the analysis due to the additional requirement of sequencing depth of the E24 sample (*P* value, exact binomial test).

the highly selective NMDA receptor antagonist 3-(2-carboxypiperazin-4-yl)propyl-1-phosphonic acid (CPP) abolished ECS-induced changes (**Fig. 3b**), confirming that these modifications are neuronal activity–dependent. Infusion of either 5-azacytidine or RG108, two mechanistically distinct DNMT inhibitors[35] previously shown to be effective in adult brains[19,21,24,26,27], abolished activity-induced *de novo* methylation with no obvious effect on demethylation (**Fig. 3b**). Notably, *Dnmt3a*, but not other *Dnmt* genes, was upregulated by ECS (**Supplementary Fig. 9**), suggesting its potential role in neuronal activity–induced *de novo* methylation. By contrast, activity-induced demethylation was abolished in *Gadd45b* knockout mice, consistent with recent findings on the critical role of Gadd45-family proteins in DNA demethylation[36]. Bisulfite sequencing of consecutive CpGs also revealed that activity-induced modifications were highly site-specific (**Fig. 3a** and **Supplementary Fig. 6a**), which may partially explain why acute methylation changes could not be readily detected by previous low-resolution profiling methods.

DNA demethylation can occur passively during cell division[4]. The adult dentate gyrus region harbors a small number of proliferating neural and glia progenitors (**Supplementary Fig. 10**). We carried out two experiments to directly test whether the observed DNA methylation changes are active in nature and independent of cell division. In the first experiment, we permanently inhibited cell proliferation in the adult hippocampus with targeted irradiation[37] (**Supplementary Fig. 10**). In the second experiment, we directly purified NeuN$^+$ postmitotic neuronal nuclei from the dentate gyrus of normal adult mice with fluorescence-activated cell sorting (FACS), which also removed potential contributions from other cell types, such as progenitors, glia and microglia (**Supplementary Fig. 11**). Similar ECS-induced CpG modifications were observed in both experiments (**Fig. 3b**), indicating that the observed CpG modification was predominantly neuronal in its origin and independent of DNA replication.

To further determine whether a physiological paradigm of neuronal stimulation could induce DNA methylation changes, we subjected adult mice to a 3-day course of voluntary running and detected highly similar changes in these regions (**Fig. 3b**). Analysis of the same set of 48 CpGs by HpaII-qPCR analysis further showed that 67% of ECS-induced methylation changes were also observed in multiple mice after running (**Fig. 4**). Thus, widespread CpG methylation changes occur in postmitotic neurons *in vivo* in response to both therapeutic and physiological neuronal activation.

Genomic characteristics of activity-modified CpGs

We next examined the genomic characteristics of the 3,050 sites identified by MSCC as differing between E4 and E0 ($\Delta_{MSCC,E4-E0}$ ≥20%).

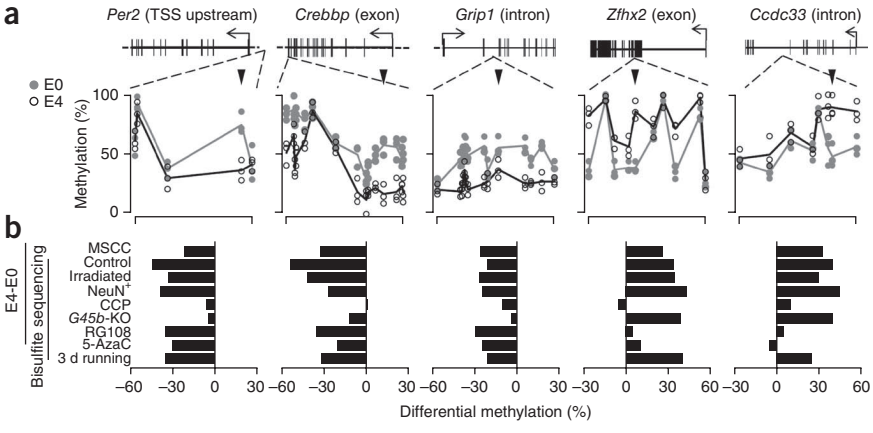

Figure 3 Biological properties of activity-induced CpG methylation changes in the adult dentate gyrus. (**a**) Examples of bisulfite sequencing analysis of CpGs in five representative regions: *Per2* (period homolog 2; demethylated in TSS upstream region; chr1:93356934–93357200), *Crebbp* (CREB binding protein; demethylated in the exon; chr16:4085747–4086068), *Grip1* (glutamate receptor interacting protein 1; demethylated in the intron; chr10:119374673–119374888), *Zfhx2* (zinc finger homeobox 2; *de novo* methylated in the exon; chr14:55691325–55691565) and *Ccdc33* (coiled-coil domain–containing 33; *de novo* methylated in the intron; chr9:57897719–57898139). Each data point represents bisulfite sequencing results from an individual mouse for these representative regions of interest at E0 (gray circles) and E4 (open circles). Lines represent mean values. Arrowheads point to MSCC sites of interest. (**b**) Summaries of methylation changes at the MSCC sites upon different manipulations (with independent corresponding controls). CCP or saline was injected 1 h before ECS. RG108, 5-azacytidine (5-AzaC) or saline was infused into the lateral ventricles 2 d before ECS. Adult male *Gadd45b* knockout (*G45b*-KO) and wild-type (Control) littermates were used, as indicated. Data represent a minimum of 20 bisulfite reads for each condition from at least two mice.

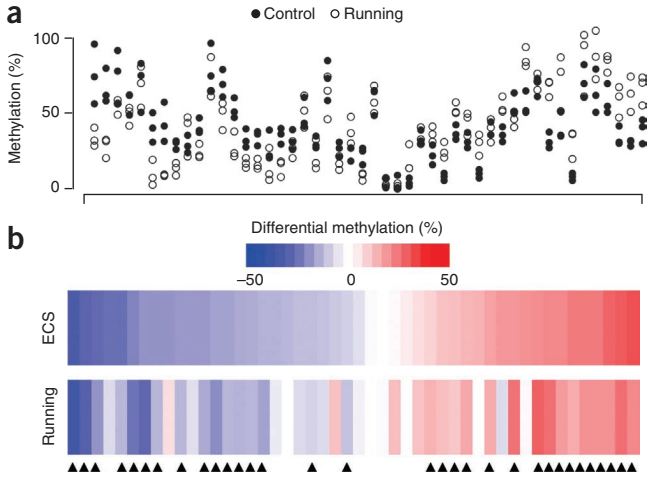

Figure 4 Voluntary exercise–induced CpG methylation changes in dentate granule cells of the adult mouse hippocampus. (**a**) Strip plot of methylation of CpGs from three control mice (filled circles) and three mice allowed to run (open circles). Adult mice were housed in standard cages with or without free access to a running wheel for 3 d. Dentate gyrus tissues were microdissected for quantification of DNA methylation with HpaII-qPCR analysis for the same set of 48 CpGs as in **Supplementary Figure 6a**. (**b**) Heat maps for mean methylation changes of the set of 48 CpGs induced by a single ECS (at 4 h) or running (after 3 d). Values represent means from three sets of mice. About 67% of CpGs examined showed similar methylation changes (arrowheads) 4 h after ECS and after 3 d of running.

Previous DNA methylation analyses have mainly focused on CpG islands, which are highly clustered CpGs often located at gene promoter regions[1,2]. Despite a modest bias of the CCGG sequence toward CpG islands, a notable exclusion of methylation changes from CpG-dense regions was observed (**Fig. 5a**), for both activity-induced *de novo* methylation and demethylation (**Supplementary Fig. 12a**). We further mapped MSCC sites to experimentally determined CpG islands[38] and observed significant resistance of both gene-associated and intergenic CpG islands from activity-induced methylation changes ($P < 2 \times 10^{-16}$; **Supplementary Fig. 12b**). Thus, low-density CpGs are main targets of activity-induced acute modifications in mature neurons *in vivo*, which is reminiscent of previously reported methylation changes during cell differentiation *in vitro*[39].

We next mapped all sites identified by MSCC to their nearby gene annotations. Unchanged and activity-modified CpGs showed substantial differences in their distribution (**Fig. 5b**). Regions downstream from the 3′ transcription end sites (TESs) were relatively depleted of MSCC sites and contributed minimally to activity-modified CpGs (4%). Activity-modified CpGs were also under-represented in 5′ regions upstream from gene TSS (putative promoters) and exonic regions but were slightly enriched in introns. Unexpectedly, intergenic CpGs (≥5 kb away from any known genes) were most susceptible to changes by neuronal activity, comprising only 10% of CpGs with no methylation changes but 38% of activity-modified CpGs ($P < 10^{-15}$; chi-squared test). Given the possibility of reactivation of DNA methylation–silenced retrotransposons in intergenic regions[40], we compared methylation patterns of 400 subclasses of repetitive elements in the mouse genome (**Supplementary Table 5**). Although most of these repetitive elements were, as expected, heavily methylated, we detected no significant changes on a global level ($\Delta_{MSCC,E4\text{-}E0} \geq 20\%$; **Supplementary Fig. 13**). It remains possible that the methylation status of individual copies of repetitive elements could be modified by neural activity.

We also compared our single-base-resolution, genome-wide neuronal DNA methylation map with activity-dependent transcription factor binding profiles recently reported for cultured mouse neurons[41]. Of note, although no significant enrichment for activity-induced methylation changes was observed, both intergenic and intragenic activity-regulated neuronal enhancers were hypomethylated in dentate granule neurons *in vivo* (**Supplementary Fig. 14a**). Furthermore, binding sites for activity-dependent transcription factors, including NPAS4 and SRF, were also hypomethylated (**Supplementary Fig. 14b**), revealing a common signature of DNA methylation at both constitutive and activity-dependent transcription factor binding sites in neurons.

Relationship between DNA methylation and gene expression

DNA methylation regulates gene expression in a highly context-dependent manner[2]. We obtained genome-wide expression profiles of dentate granule neurons at E0 and E4 using a mouse exon microarray (**Supplementary Table 6**). Integrated analysis comparing the relationship between genome-wide CpG methylation and gene expression in previously characterized cell types, including MSCC-profiled human B lymphocytes[7] and MethylC-seq (whole-genome bisulfite sequencing)-profiled human embryonic stem cells[34], revealed a distinct epigenetic pattern in the adult mouse dentate granule neurons *in vivo* (**Supplementary Fig. 15a**). Like that in other cell types, CpG methylation near TSSs in dentate granule neurons was anticorrelated with the gene expression. Unexpectedly, however, the previously observed positive correlation between gene body CpG methylation and gene expression was absent in these neurons. The anticorrelation between CpG methylation and gene expression extended throughout the whole gene body into the 3′ regions downstream from TESs. Furthermore, the robust anticorrelation was strongly dependent on low-density CpGs (**Supplementary Fig. 15b**), suggesting that the role of low-density CpGs in regulating gene expression may have been previously underappreciated[42].

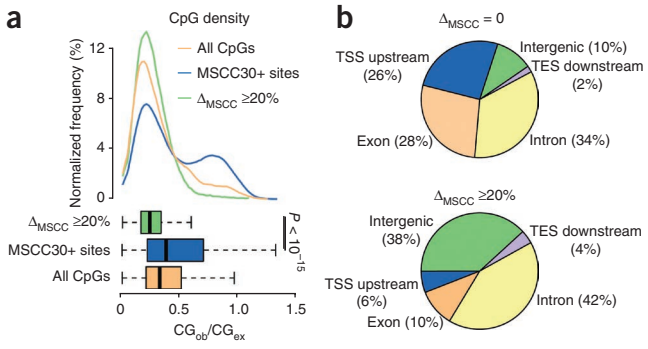

Figure 5 Genomic characteristics of activity-modified CpGs. (**a**) Enrichment of activity-induced methylation changes in regions with low CpG density. Top: distributions of CpG densities of 500-bp windows flanking activity-modified CpGs, all MSCC sites with ≥30 reads (MSCC30+ sites) and all CpGs in the mouse genome; Bottom: box plots showing median and quartiles of the three distributions (CG_{ob}, observed CpG number; CG_{ex}, expected CpG number; *P* value, Student's *t*-test). (**b**) Distribution of modified CpGs in different genomic subregions. Charts show unchanged (top) and activity-modified CpGs (bottom) mapped to each genomic subregion. TSS upstream, within 5 kb upstream from the TSS; TES downstream, within 5 kb downstream from the TES; intergenic, >5 kb away from any known gene.

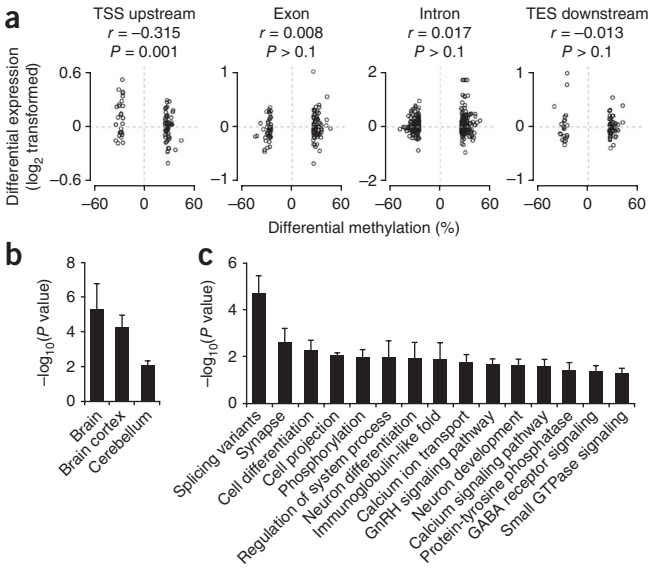

Figure 6 Correlation between changes in CpG methylation and gene expression, and enrichment of activity-modified CpGs in brain-specific genes and neuronal pathways. (**a**) Correlation between activity-induced methylation changes of CpGs in different genomic subregions and mRNA level changes of associated genes between E4 and E0 (*P* values, Pearson's correlation test). (**b**,**c**) Tissue-specific expression (**b**) and gene ontology (GO) analysis (**c**) of genes associated with activity-modified CpGs. Only nonredundant GO terms are shown in **c**. To control for the gene length effect, only GO terms that show *P* values less than 0.1 (Fisher's exact test) using each of the three independent random CpG sets generated from all MSCC sites with sequencing depth ≥30 are shown.

Although activity-modified CpGs were enriched in intergenic regions, 1,819 activity-modified CpGs mapped to 1,518 genes (**Supplementary Table 7**). We next determined whether activity-induced changes in CpG methylation correlated with changes in the expression of associated genes. The methylation changes located in TSS upstream regions (putative promoters) were modestly but significantly anticorrelated with changes in gene expression (**Fig. 6a**). We confirmed the results using quantitative real-time PCR analysis of multiple individual mice (**Supplementary Fig. 16** and **Supplementary Table 8**). In contrast, we detected no significant correlation between methylation changes in other gene structures and gene expression changes (**Fig. 6a**). These results support the notion that activity-induced methylation changes may regulate gene expression in a highly context-dependent manner and may function other than through directly regulating transcription levels. Our finding resembles the lack of correlation between active DNA modifications and gene expression changes observed during differentiation of human peripheral blood monocytes[43].

Activity-modified CpGs are enriched in brain genes

Finally, we examined the characteristics of the 1,518 genes associated with the activity-modified 1,819 CpGs. Using three randomly generated gene sets as the background to control for any gene length effects, the 1,518 genes were significantly enriched in genes that are expressed in the brain (**Fig. 6b**). Activity-modified CpGs were also preferentially associated with alternative splicing variants (**Fig. 6c**), suggesting a potential role of DNA methylation changes in regulating alternative splicing in neurons.

Gene ontology analysis revealed significant over-representations of genes involved in synaptic function, protein phosphorylation, neuronal differentiation and the calcium signaling pathway (**Fig. 6c**, **Supplementary Figs. 17–19** and **Supplementary Table 9**), some of which were also enriched at the mRNA level in activity-regulated genes (**Supplementary Fig. 20**). Unexpectedly, several genes encoding Notch signaling components showed CpG methylation and gene expression changes (**Supplementary Fig. 21**). Identification of the Notch signaling pathway as an epigenetic target of neuronal activity in mature neurons supports its emerging role in synaptic plasticity and long-term memory[44].

DISCUSSION

Our study shows how the epigenetic DNA methylation landscape of mature neurons is rapidly modified in response to external stimuli *in vivo*. Recent technical advances have enabled accurate and large-scale profiling of CpG methylation status across the mammalian genome[7,33,34,39]. In contrast to previous studies that have compared different mammalian cell types *in vitro*[7,33,39] or mainly focused on CpGs within promoter regions in heterogeneous tissues[45], we describe to our knowledge the first genome-wide, quantitative characterization of activity-induced acute CpG methylation changes for a defined mature neuronal subtype *in vivo*. Together with the gene expression profiles, these data sets will serve as a resource for the neuroscience community. The adult dentate gyrus provides a relatively homogenous population of postmitotic neurons that can be activated synchronously *in vivo* and are readily available in large numbers[17]. Such properties are particularly important for epigenetic analysis because each diploid cell contains only two locus-specific modifications.

Our study reveals several key aspects of activity-induced epigenetic DNA modifications. First, our result provides direct evidence that extensive active DNA modifications occur in mature neurons *in vivo*, including DNA demethylation and *de novo* methylation. An appreciable subset of CpGs (~1.4%) in the genome of mature neurons is acutely modified in a site-specific fashion in response to various stimuli, including behavioral stimulation. Second, our analysis reveals new characteristics of the genomic distribution of activity-induced DNA modifications in mature neurons *in vivo* (**Supplementary Fig. 22**). Highly clustered CpGs form CpG islands around TSSs of genes and are mostly unmethylated in the basal state. CpG island–associated hypermethylation often occurs at tumor suppressor gene promoters in cancer[46]. Recent studies have also identified a subset of CpGs located near CpG islands, named CpG shores[45], that are subject to tissue-specific and/or cancer-related methylation. In contrast, activity-modified CpGs reside mostly in low-CpG-density regions and in both intragenic and intergenic regions, resembling aging-associated CpG methylation changes in liver cells[47]. Third, our study identifies many genes and pathways that are subject to modulation by neuronal activity at the level of DNA modification, including some, such as the Notch signaling pathway, that are not traditionally associated with mature neuronal functions.

Our findings are supported by the continuous expression of DNMTs and putative DNA demethylation machinery genes (for example, *Gadd45*, *Tdg* (thymine DNA glycosylase), *Tet* oxygenases and *Mbd4* (methyl-CpG binding domain protein 4)) in the adult brain[3,9,48]. Indeed, activity-induced *de novo* CpG methylation requires DNMT activity, consistent with recent genetic studies that identified a critical role of the persistent expression of these enzymes in activity-dependent neuronal plasticity[20]. We confirmed our previous finding that Gadd45b is essential for activity-induced DNA demethylation[17]. The recent discovery of the TET proteins as mammalian 5mC hydroxylases has raised interest in the potential role of TET-catalyzed 5mC

hydroxylation in active DNA demethylation[4,9]. Of note, 5hmCs, the product of 5mC hydroxylation, are abundant in the adult dentate gyrus[48]. We recently showed that Tet1 is required for activity-induced demethylation of *Bdnf IX* and *Fgf1 B* promoters in adult dentate granule cells *in vivo*[48]. Because bisulfite sequencing and most methylation-sensitive restriction enzymes cannot distinguish 5mC and 5hmC (ref. 48), new high-throughput methods to profile 5hmCs at the genome scale with single-nucleotide resolution need to be developed.

Emerging evidence suggests that DNA modification regulates gene transcription in a highly context-dependent manner[2]. Densely methylated CpG islands are known to repress gene transcription[1,2], whereas methylation in adjacent CpG shores has been shown to be more widely anticorrelated with tissue-specific gene expression[45] (**Supplementary Fig. 22**). In some cases, low-density CpGs in regulatory regions also can repress transcription[49]. In contrast, recent epigenomic studies have suggested a function of gene body methylation in transcriptional activation[7,8]. Furthermore, 5hmCs are intermediate products of DNA demethylation[48], but they may independently also regulate gene expression[9]. Our integrated analysis of the single-base-resolution DNA methylome and the genome-wide expression profile of endogenous neurons revealed a distinct relationship between gene body methylation and gene expression, compared with other previously profiled cell types[7,34]. Given the high site specificity, the broad genomic distribution and the enrichment in intergenic and low CpG-density regions, activity-induced CpG methylation changes alone may not be sufficient for transcriptional control of their associated genes. Indeed, only CpG modifications in TSS upstream regions were modestly anticorrelated with gene expression changes. Thus, transcriptional control may require not only DNA methylation changes but also coordination with transcription factor binding and histone modifications. Neuronal activity–induced DNA modification could thus provide a permissive condition for other activity-dependent events that eventually lead to changes in the level, duration and/or isoforms of gene expression. It will be interesting to determine the potential function of both intergenic and intragenic activity-modified CpGs in the future.

The scope and specificity of activity-induced, relatively sustained DNA modifications *in vivo* suggest that such epigenetic regulation can serve as a general mechanism for activity-induced epigenetic control and long-lasting plasticity in neurons. Thus, in addition to histone modifications and transcription factors, epigenetic DNA modifications may expand the capacity of mature neurons to perpetuate transient stimuli into long-lasting covalent modifications in the nucleus. The MSCC method provides a cost-effective and single-base-resolution method for digital profiling of CpG methylation across the whole genome and can be readily applied to other biological conditions. Given suggested roles of epigenetic aberrations in aging, neurological and psychiatric disorders[3,10], the inducible reversibility of epigenetic DNA methylation in the adult brain by neuronal activation and behavioral stimulation offers the possibility for new kinds of therapies.

METHODS

Methods and any associated references are available in the online version of the paper at http://www.nature.com/natureneuroscience/.

Accession codes. Gene Expression Omnibus: GSE30493.

Note: Supplementary information is available on the Nature Neuroscience website.

ACKNOWLEDGMENTS

We thank G. Church, S. Baylin, D. Ginty and K. Christian for comments and suggestions; G. Sun for help with FACS; and W.Y. Kim (Johns Hopkins University) for breeding *Gadd45b* knockout mice. This work was supported by US National Institutes of Health (NIH; AG024984, NS047344), McKnight Scholar Award and NARSAD (Brain and Behavior Research Fund) to H.S.; by NIH (HD069184, NS048271), Johns Hopkins Brain Science Institute, Dr. Miriam and Sheldon G. Adelson Medical Research Foundation, and NARSAD grants to G.-l.M.; and Lieber Institute start-up funds to Y.G. J.U.G. was a FARMS (Foundation for Advanced Research in Medical Sciences) fellow. M.H.J. was supported by a US National Institute of Mental Health K99 award (MH090115). M.A.B. was partially supported by a fellowship from Maryland Stem Cell Research Fund (MSCRF); M.P.B. was supported by grants from the NIH to G. Church.

AUTHOR CONTRIBUTIONS

J.U.G., D.K.M., G.M., Y.G. and H.S. designed the project. J.U.G. led and was involved in all aspect of the project. H.M. performed sequence mapping and methylation calculation. M.P.B. constructed libraries and performed initial methylation analysis. M.-H.J. assisted in BrdU analysis, irradiation and drug infusion procedures. M.A.B. performed FACS purification. J.A.B. wrote the gene mapping program. H.L.E. adapted MOM for the current project. B.X. and H.M. performed Illumina sequencing. E.F. contributed to irradiation studies. K.Z. contributed to data processing. J.U.G., G.M., Y.G. and H.S. wrote the paper.

COMPETING FINANCIAL INTERESTS

The authors declare no competing financial interests.

Published online at http://www.nature.com/natureneuroscience/.
Reprints and permissions information is available online at http://www.nature.com/reprints/index.html.

1. Reik, W. Stability and flexibility of epigenetic gene regulation in mammalian development. *Nature* **447**, 425–432 (2007).
2. Suzuki, M.M. & Bird, A. DNA methylation landscapes: provocative insights from epigenomics. *Nat. Rev. Genet.* **9**, 465–476 (2008).
3. Ma, D.K. *et al.* Epigenetic choreographers of neurogenesis in the adult mammalian brain. *Nat. Neurosci.* **13**, 1338–1344 (2010).
4. Wu, S.C. & Zhang, Y. Active DNA demethylation: many roads lead to Rome. *Nat. Rev. Mol. Cell Biol.* **11**, 607–620 (2010).
5. Zemach, A., McDaniel, I.E., Silva, P. & Zilberman, D. Genome-wide evolutionary analysis of eukaryotic DNA methylation. *Science* **328**, 916–919 (2010).
6. Hellman, A. & Chess, A. Gene body-specific methylation on the active X chromosome. *Science* **315**, 1141–1143 (2007).
7. Ball, M.P. *et al.* Targeted and genome-scale strategies reveal gene-body methylation signatures in human cells. *Nat. Biotechnol.* **27**, 361–368 (2009).
8. Wu, H. *et al.* Dnmt3a-dependent nonpromoter DNA methylation facilitates transcription of neurogenic genes. *Science* **329**, 444–448 (2010).
9. Guo, J.U., Su, Y., Zhong, C., Ming, G.L. & Song, H. Emerging roles of TET proteins and 5-hydroxymethylcytosines in active DNA demethylation and beyond. *Cell Cycle* **10**, 2662–2668 (2011).
10. Tsankova, N., Renthal, W., Kumar, A. & Nestler, E.J. Epigenetic regulation in psychiatric disorders. *Nat. Rev. Neurosci.* **8**, 355–367 (2007).
11. Borrelli, E., Nestler, E.J., Allis, C.D. & Sassone-Corsi, P. Decoding the epigenetic language of neuronal plasticity. *Neuron* **60**, 961–974 (2008).
12. Szyf, M., McGowan, P. & Meaney, M.J. The social environment and the epigenome. *Environ. Mol. Mutagen.* **49**, 46–60 (2008).
13. Day, J.J. & Sweatt, J.D. DNA methylation and memory formation. *Nat. Neurosci.* **13**, 1319–1323 (2010).
14. Guan, J.S. *et al.* HDAC2 negatively regulates memory formation and synaptic plasticity. *Nature* **459**, 55–60 (2009).
15. Doi, M., Hirayama, J. & Sassone-Corsi, P. Circadian regulator CLOCK is a histone acetyltransferase. *Cell* **125**, 497–508 (2006).
16. Maze, I. *et al.* Essential role of the histone methyltransferase G9a in cocaine-induced plasticity. *Science* **327**, 213–216 (2010).
17. Ma, D.K. *et al.* Neuronal activity-induced Gadd45b promotes epigenetic DNA demethylation and adult neurogenesis. *Science* **323**, 1074–1077 (2009).
18. Nelson, E.D., Kavalali, E.T. & Monteggia, L.M. Activity-dependent suppression of miniature neurotransmission through the regulation of DNA methylation. *J. Neurosci.* **28**, 395–406 (2008).
19. Miller, C.A. *et al.* Cortical DNA methylation maintains remote memory. *Nat. Neurosci.* **13**, 664–666 (2010).
20. Feng, J. *et al.* Dnmt1 and Dnmt3a maintain DNA methylation and regulate synaptic function in adult forebrain neurons. *Nat. Neurosci.* **13**, 423–430 (2010).
21. LaPlant, Q. *et al.* Dnmt3a regulates emotional behavior and spine plasticity in the nucleus accumbens. *Nat. Neurosci.* **13**, 1137–1143 (2010).
22. Martinowich, K. *et al.* DNA methylation-related chromatin remodeling in activity-dependent BDNF gene regulation. *Science* **302**, 890–893 (2003).
23. Weaver, I.C. *et al.* Epigenetic programming by maternal behavior. *Nat. Neurosci.* **7**, 847–854 (2004).
24. Miller, C.A. & Sweatt, J.D. Covalent modification of DNA regulates memory formation. *Neuron* **53**, 857–869 (2007).

25. Dong, E., Nelson, M., Grayson, D.R., Costa, E. & Guidotti, A. Clozapine and sulpiride but not haloperidol or olanzapine activate brain DNA demethylation. *Proc. Natl. Acad. Sci. USA* **105**, 13614–13619 (2008).
26. Lubin, F.D., Roth, T.L. & Sweatt, J.D. Epigenetic regulation of BDNF gene transcription in the consolidation of fear memory. *J. Neurosci.* **28**, 10576–10586 (2008).
27. Elliott, E., Ezra-Nevo, G., Regev, L., Neufeld-Cohen, A. & Chen, A. Resilience to social stress coincides with functional DNA methylation of the *Crf* gene in adult mice. *Nat. Neurosci.* **13**, 1351–1353 (2010).
28. Murgatroyd, C. *et al.* Dynamic DNA methylation programs persistent adverse effects of early-life stress. *Nat. Neurosci.* **12**, 1559–1566 (2009).
29. McGowan, P.O. *et al.* Epigenetic regulation of the glucocorticoid receptor in human brain associates with childhood abuse. *Nat. Neurosci.* **12**, 342–348 (2009).
30. Lisanby, S.H. Electroconvulsive therapy for depression. *N. Engl. J. Med.* **357**, 1939–1945 (2007).
31. Shock, L.S., Thakkar, P.V., Peterson, E.J., Moran, R.G. & Taylor, S.M. DNA methyltransferase 1, cytosine methylation, and cytosine hydroxymethylation in mammalian mitochondria. *Proc. Natl. Acad. Sci. USA* **108**, 3630–3635 (2011).
32. Nass, M.M. Differential methylation of mitochondrial and nuclear DNA in cultured mouse, hamster and virus-transformed hamster cells. In vivo and in vitro methylation. *J. Mol. Biol.* **80**, 155–175 (1973).
33. Laurent, L. *et al.* Dynamic changes in the human methylome during differentiation. *Genome Res.* **20**, 320–331 (2010).
34. Lister, R. *et al.* Human DNA methylomes at base resolution show widespread epigenomic differences. *Nature* **462**, 315–322 (2009).
35. Stresemann, C., Brueckner, B., Musch, T., Stopper, H. & Lyko, F. Functional diversity of DNA methyltransferase inhibitors in human cancer cell lines. *Cancer Res.* **66**, 2794–2800 (2006).
36. Ma, D.K., Guo, J.U., Ming, G.L. & Song, H. DNA excision repair proteins and Gadd45 as molecular players for active DNA demethylation. *Cell Cycle* **8**, 1526–1531 (2009).
37. Ford, E.C. *et al.* Localized CT-guided irradiation inhibits neurogenesis in specific regions of the adult mouse brain. *Radiat. Res.* **175**, 774–783 (2011).
38. Illingworth, R.S. *et al.* Orphan CpG islands identify numerous conserved promoters in the mammalian genome. *PLoS Genet.* **6**, e1001134 (2010).
39. Meissner, A. *et al.* Genome-scale DNA methylation maps of pluripotent and differentiated cells. *Nature* **454**, 766–770 (2008).
40. Muotri, A.R. *et al.* Somatic mosaicism in neuronal precursor cells mediated by L1 retrotransposition. *Nature* **435**, 903–910 (2005).
41. Kim, T.K. *et al.* Widespread transcription at neuronal activity-regulated enhancers. *Nature* **465**, 182–187 (2010).
42. Weber, M. *et al.* Distribution, silencing potential and evolutionary impact of promoter DNA methylation in the human genome. *Nat. Genet.* **39**, 457–466 (2007).
43. Klug, M. *et al.* Active DNA demethylation in human postmitotic cells correlates with activating histone modifications, but not transcription levels. *Genome Biol.* **11**, R63 (2010).
44. Pierfelice, T., Alberi, L. & Gaiano, N. Notch in the vertebrate nervous system: an old dog with new tricks. *Neuron* **69**, 840–855 (2011).
45. Irizarry, R.A. *et al.* The human colon cancer methylome shows similar hypo- and hypermethylation at conserved tissue-specific CpG island shores. *Nat. Genet.* **41**, 178–186 (2009).
46. Herman, J.G. & Baylin, S.B. Gene silencing in cancer in association with promoter hypermethylation. *N. Engl. J. Med.* **349**, 2042–2054 (2003).
47. Thompson, R.F. *et al.* Tissue-specific dysregulation of DNA methylation in aging. *Aging Cell* **9**, 506–518 (2010).
48. Guo, J.U., Su, Y., Zhong, C., Ming, G.L. & Song, H. Hydroxylation of 5-methylcytosine by TET1 promotes active DNA demethylation in the adult brain. *Cell* **145**, 423–434 (2011).
49. Simonsson, S. & Gurdon, J. DNA demethylation is necessary for the epigenetic reprogramming of somatic cell nuclei. *Nat. Cell Biol.* **6**, 984–990 (2004).

ONLINE METHODS

Biological samples. Adult mice (wild-type and *Gadd45b* knockout, 8–10 weeks old, male, C57BL/6 background) were housed in a standard facility. All animal procedures used in this study were performed in accordance with protocols approved by the Institutional Animal Care and Use Committee of Johns Hopkins University. ECS was administered with 1.0-s stimuli (total duration) consisting of 100 Hz, 18 mA, 0.3-ms pulses delivered using a Ugo Basile ECT unit (model 57800) as previously described[17]. Sham-treated mice (E0) were similarly handled in parallel without the current delivery. Previous studies did not find any detectable damage resulting from ECS[17], through assays including western blot and immunostaining of the activated form of caspase (Caspase 3a) and phosphorylated ATM (ataxia telangiectasia mutated kinase). In one set of experiments, CPP (10 mg kg^{-1}, intraperitoneal) was injected 1 h before ECS to block NMDA receptors. In another set of experiments, osmotic pumps (flow rate 1.0 µl h^{-1}, pre-equilibrated in saline at 37 °C overnight; Alzet model 1003D) were implanted to deliver one of two structurally different DNMT inhibitors[35], RG108 (1 mM; Sigma) and 5-azacytidine (1 mM; Sigma), or saline into one side of brain ventricles 2 d before ECS or sham treatment. Only ipsilateral dentate gyri from infusion experiments were used for DNA methylation analysis. In experiments with voluntary exercise (running) for 3 d, adult mice were randomly separated into two groups in standard home cages with or without free access to a mounted running wheel as described previously[17].

To eliminate proliferating cells in the adult dentate gyrus, targeted irradiation at the hippocampus region was carried out as previously described[37]. Sham and irradiated mice were allowed to recover for 5 weeks before use, when no difference in microglia numbers or activation was detected between sham and irradiated mice (**Supplementary Fig. 10**). To examine the status of DNA replication in the dentate gyrus of treated mice at the time of use, mice were injected with BrdU (200 mg kg^{-1}, intraperitoneal) and killed 2 h later. Coronal brain sections (40 µm thick) were prepared and processed for immunostaining using antibodies to BrdU (rat; 1:400; Accurate) as previously described[17]. Images were acquired on an LSM 510 Live confocal system (Carl Zeiss). Stereological quantification of $BrdU^+$ cells within the subgranular zone and granule cell layer was carried out as previously described[17] (**Supplementary Fig. 10**).

Dentate gyrus tissues were rapidly microdissected bilaterally from adult mice unless specified. Immunohistology shows that such preparations contain ~90% $NeuN^+$ neurons[17]. Each MSCC sample contained pooled DNA from two mice (four dentate gyri). All validation experiments were performed using independent biological samples of bilaterally microdissected dentate gyri from individual mice.

In some experiments, FACS was used to further enrich the postmitotic neuronal population and remove the potential contribution from glia, progenitors and other non-neuronal cell types (**Supplementary Fig. 11**). Briefly, dentate gyrus tissues were removed from mice receiving ECS or sham treatment, flash-frozen in a mix of dry ice powder with 100% ethanol and transferred to −80 °C for at least overnight. Tissue from each condition was pooled and homogenized on ice using a Dounce homogenizer (Fisher) in lysis buffer containing 0.32 M sucrose, 5 mM $CaCl_2$, 3 mM magnesium diacetate, 0.1 mM EDTA, 10 mM Tris-HCl, pH 8.0, 1 mM DTT (Roche) and 0.1% Triton X-100 for 1 min. The cell lysate was then loaded onto a sucrose gradient containing 1.8 mM sucrose, 3 mM magnesium diacetate, 10 mM Tris-HCl, pH 8.0, and 1 mM DTT, and centrifuged for 2.5 h at 26,000 r.p.m. (SW32Ti rotor) at 4 °C (Beckman Coulter). The supernatant containing cell debris was aspirated and 500 µl of PBS was added to the nuclear pellet. After 20 min on ice, the nuclear pellet was resuspended in PBS with gentle trituration. An immunostaining mixture containing 195 µl PBS with 0.6 µl antibodies to NeuN (Millipore), 1 µl R-phycoerythrin (Invitrogen) and 5 µl normal goat sera was briefly mixed, incubated for 5 min and applied to the nuclei for 45 min in the dark. Control reactions were performed by omitting the primary antibody (negative control) and by adding 2 µg ml^{-1} 7-aminoactinomycin D (Sigma) as a nuclear counterstain (positive control). After incubation, stained nuclei were gently triturated and passed through a 40-µm filter into sorting tubes. Control samples were then used to determine the forward-scatter and side-scatter nuclear profiles and background phycoerythrin gating. $NeuN^+$ nuclei from sham and ECS samples were purified using the FACSVantage SE (BD) into PBS according to forward-scatter, side-scatter and phycoerythrin profiles. FACS profiles were processed using CellQuest software (BD). Lysis buffer was directly added to purified nuclei and genomic DNA collected as previously described[17]. To verify FACS samples by immunofluorescence microscopy, the nuclear counterstain DAPI was added (2 µg ml^{-1}) to a $NeuN^+$ sample after sorting.

MSCC library construction, sequencing, mapping and data analysis. Genomic DNA was extracted and purified using Qiagen DNeasy Kit as previously described[17]. Concentrations and 260-nm/280-nm UV absorbance ratios were determined by Thermo NanoDrop2000 to ensure the sample quality. Typically, 1.5–2.5 µg genomic DNA could be obtained from each dentate gyrus. For each sample, four dentate gyri from two mice were pooled to increase the sample concentration and diminish microdissection variations.

MSCC[7] characterizes CpG methylation status across the genome by using two restriction enzymes, the methylation-sensitive HpaII and the methylation-insensitive isoschizomer MspI. Both enzymes target the same CCGG sequence. HpaII cuts unmethylated CCGG sites but not methylated or hydroxymethylated ones, whereas MspI cuts all CCGG sites. Sequencing read counts mapped to HpaII and MspI cut sites provide quantitative and digital measurement of CpG methylation within the CCGG site. For the improved MSCC method (**Supplementary Fig. 2**), two libraries were constructed for each DNA sample, an HpaII library and an inverse library, as previously described[7]. Briefly, two custom adaptors were synthesized by IDT. Adaptor A contained a 5′ MmeI recognition site and a 5′ CG overhang, whereas adaptor B contained a 3′ NN (where N is A, T, C or G) overhang. Both adaptors also contained end sequences required by Illumina library construction. For the HpaII Library, 2 µg of genomic DNA was digested with HpaII. Adaptor A was ligated to HpaII-digested fragments. After digestion with MmeI, the resulting fragments were ligated to adaptor B. The final library fragments were then purified using a 6% polyacrylamide gel. For the inverse library, after DNA was digested with HpaII, the fragment ends were deactivated by treating with Antarctic Phosphatase (NEB). Then DNA was digested by MspI, purified and treated in the same manner as for the HpaII library. After sequencing, the number of sequencing reads matched to a site from HpaII library came from the unmethylated sites; the number of sequencing reads matched to a site from the inverse library came from the methylated or hydroxymethylated sites. Standard DNA with artificially introduced methylation levels was used to normalize the counts before estimating the methylation.

For sequencing read alignment, a set of possible 17- and 18-bp tags was created from all CCGG sites in the mouse genome (mm9, downloaded from the UCSC genome browser (http://genome.ucsc.edu/)). Our custom, Java-based software MOM was used to match sequencing reads to the set of tags[50]. Sequencing reads that could be mapped uniquely with up to one mismatch were tallied for each location and then used to calculate methylation percentage by the following formula as previously described[7]:

$$\text{methylation percentage} = 100\% \times \text{count}_{\text{inverse-library}} / (\text{ratio} \times \text{count}_{\text{HpaII-library}} + \text{count}_{\text{inverse-library}})$$

where ratio = $\text{count}_{\text{inverse-standard}}/\text{count}_{\text{HpaII-standard}}$. CpG sites with low counts (for example, inverse + HpaII <30 counts) were excluded from further analysis.

R packages (http://www.r-project.org/) were used for all bioinformatic analysis unless specified. For CpG density calculation, 500-bp flanking sequences were fetched from mouse genome (mm9) for different subsets of MSCC sites. CpG density was calculated by the following formula:

$$\text{CpG}_{\text{observed}}/\text{CpG}_{\text{expected}} = \text{CpG}_{\text{observed}}/[\text{length} \times p(C) \times p(G)]$$

where p(C) and p(G) denote the percentage of Cs and Gs in the sequence, respectively.

For functional annotation, MSCC sites were mapped to known genes using relevant tables from the UCSC genome browser by in-house programs. Tissue specificity and gene ontology analysis were done using DAVID (http://david.abcc.ncifcrf.gov/). Three independent, equal-sized gene sets were generated from all MSCC sites having a sequencing depth ≥30 as background sets to control for the gene length effect.

Bisulfite sequencing and HpaII-qPCR analysis. For bisulfite sequencing analysis, 1 µg of genomic DNA was treated with sodium bisulfite (Zymo) as previously described[17]. Sodium bisulfite converts unmethylated cytosines to uracils, whereas 5-methylcytosines and 5hmCs remain unconverted. The converted DNA

doi:10.1038/nn.2900

was purified and 50 ng was used as the template in a 50-µl PCR reaction using Choice-Taq polymerase (Denville). Specific primers were designed to amplify regions of interest (listed in **Supplementary Table 2**). Fresh PCR products were purified (Qiagen), cloned by the TOPO-TA cloning method (Invitrogen) and sequenced. Unmethylated cytosines appear as thymines and methylated cytosines appear as cytosines. The efficiency of bisulfite conversion is confirmed by the complete conversion of non–CG cytosines to thymines in PCR-amplified sequences. We considered a difference of ≥20% in bisulfite sequencing to be a true difference in calculation of specificity and sensitivity of MSCC at different cutoffs by the following formulas:

$$\text{specificity} = 100\% \times \text{count}_{\text{true-positive}}/(\text{count}_{\text{true-positive}} + \text{count}_{\text{false-positive}})$$
$$\text{sensitivity} = 100\% \times \text{count}_{\text{true-positive}}/(\text{count}_{\text{true-positive}} + \text{count}_{\text{false-negative}})$$

For HpaII-based methylation-sensitive qPCR analysis, 1 µg of genomic DNA was mock treated or was digested by HpaII or MspI for at least 4 h. After heat inactivation at 80 °C for 20 min, the same volumes of reaction products were taken as templates for qPCR with primers flanking the restriction sites (**Supplementary Table 3**). The HpaII-resistant fraction was calculated as $2^{[\text{Ct(undigested)} - \text{Ct(HpaII)}]}$. Less than 5% of the sample was MspI resistant, confirming the PCR specificity.

Expression profiling and bioinformatic analysis. Total RNA was extracted by TRIzol reagent (Invitrogen) and further purified by RNeasy columns (Qiagen). Processing, labeling, hybridization and intensity acquisition was performed by the Johns Hopkins Microarray Core Facility using standard protocols for the Affymetrix GeneChip Mouse Exon 1.0ST array. Two biological replicates were performed for both E0 and E4. Preprocessing of raw data files was performed using the "oligo" package in R. Raw intensities were $\log_2$-transformed, background-corrected and quantile-normalized by robust multi-array analysis (RMA). Probe set information was downloaded from the Affymetrix website. Using Refseq tables from the UCSC Genome Browser, all nonexonic probe sets were filtered out. Next, all exonic probe sets within each Refseq transcript were averaged to obtain the gene-level expression values (**Supplementary Table 6**). To correlate CpG methylation and gene expression, relative distance of each MSCC site to its nearby gene(s) was calculated. The relative distance is represented by a value between −0.5 to 1.5. Values between −0.5 and 0 represent 5,000 to 0 bp upstream from the TSS. Values between 0 and 1 represent 0 to 100% of the distance along the gene body. Values between 1 and 1.5 represent 0 to 5,000 bp downstream from the TES. A moving window of 0.1 for relative distance was used to calculate averaged methylation for genes with different expression levels or to calculate Spearman's correlations of all sites within the window. To calculate the correlation between methylation changes and expression changes, MSCC sites of $\Delta_{\text{MSCC}} \geq 25\%$ were used. For pathway analysis, genes with differential expression ≥0.5 were used.

50. Eaves, H.L. & Gao, Y. MOM: maximum oligonucleotide mapping. *Bioinformatics* **25**, 969–970 (2009).